Monitoring of hydrogen concentration using capacitive nanosensor in a 1% H_2–N_2 mixture

Ghobad Behzadi Pour ✉, *Leila Fekri Aval*

Department of Physics, East Tehran Branch, Islamic Azad University, Tehran, Iran
✉ *E-mail: ghobadbehzadi@yahoo.com*

Published in Micro & Nano Letters; Received on 7th August 2017; Accepted on 1st September 2017

In this work, a hydrogen capacitor nanosensor with palladium nanoparticles (PdNPs) electrode based on metal–oxide–semiconductor structure has been fabricated. The capacitor sensor has been fabricated on the n-type silicon substrate with an oxide film thickness of 50 nm. PdNPs are synthesised and then deposited on the oxide surface using spin coating. PdNPs are characterised using by transmission electron microscope and UV spectrum. Also, the morphology of the oxide surface is characterised using by atomic force microscope. The response time and recovery time of nanosensor have been explained at the room temperature. The time interval to 90% of the signal value for 1% H_2–N_2 mixture was 1.4 s and recovery time was 14 s. The curve of pressure as a function of hydrogen concentration (H/Pd) in the PdNPs and the mechanism of the nanosensor are reported. The capacitor nanosensor based on nanoparticles shows sensitive and fast response.

1. Introduction: Hydrogen is a tasteless and flammable gas that is cannot be detected without sensor. Hubert *et al.* [1] described the different types of hydrogen sensors in different structures and detection limits. Sensitive and faster hydrogen gas sensors are required in many industries. The largest application of hydrogen is for the processing of fossil fuels and in the production of ammonia. The detection of hydrogen leaks before concentration rises above the lower flammability limit in air is necessary during in both automotive and stationary applications, chemical, power generation and telecommunications industries. In more recent applications, hydrogen is used pure or mixed with nitrogen as a tracer gas for leak detection [2, 3]. Hydrogen sensor is a transducer device that detects the presence of hydrogen molecules and produce an electrical signal. They are used to locate hydrogen leaks and considered faster. There are eight types of hydrogen and palladium (Pd) are used in many of these. Pd absorbs hydrogen atom and forms the compound palladium hydride [4, 5].

Capacitive sensors are transducer devices that detect changes in environment and produce an electrical signal. These sensors convert the signals to the electrical capacitance and electrical conductivity. Capacitive sensors are used in gas detection and measurement of electrical properties of different water liquids [6–10]. Hydrogen sensors based on metal–oxide–semiconductor (MOS) structure were first reported by Lundstrom *et al.* in 1975 [11]. In capacitor hydrogen sensor with MOS structure, hydrogen atoms at the gate/SiO_2 interface giving rise to a dipole layer. In the capacitor hydrogen sensor, the basic principle is based on the shift in the flat-band voltage (V_{FB}). The Ni, Pt and Pd thin films and their composites with carbon nanotubes, graphene, quantum dots and nanowires are used in sensors [12–14]. In this Letter, a hydrogen nanosensor based on the Pd nanoparticles (PdNPs) MOS capacitor has been reported. The synthesis and characterisation of PdNPs and also the mechanism of the nanosensor for hydrogen concentration are presented. The response and recovery speed of the MOS hydrogen sensor based on nanoparticles are found very fast compare to other ultrathin film MOS hydrogen sensors.

2. Material and methods: The nanoparticles by chemical method using a Pd chloride ($PdCl_2$) (0.2 g), pectin (2 g), gelatin (2 g) and distilled water (300 ml) are synthesised. The gelatin is used as a reductant for PdNPs [13]. The mixture of $PdCl_2$, pectin, gelatin and distilled is shown in Fig. 1*a*. Fig. 1*b* shows the TEM images of the PdNPs. The average size of PdNPs is 9 nm.

The UV spectrum of PdNPs at the room temperature is shown in Fig. 2. The UV spectra of $PdCl_2$ before and after reduction are shown in [15–17]. The UV spectra show $PdCl_2$ is converted to PdNPs.

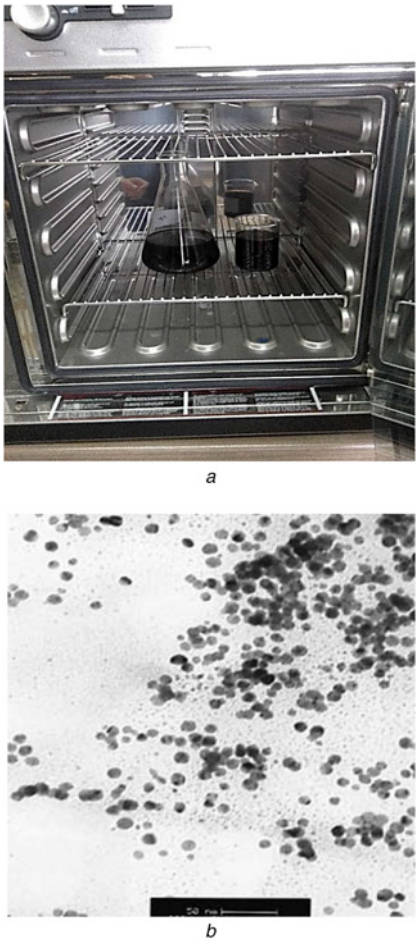

Fig. 1 *Mixture of $PdCl_2$, pectin, gelatin and distilled water*
a Dark-grey solution
b TEM images of the PdNPs

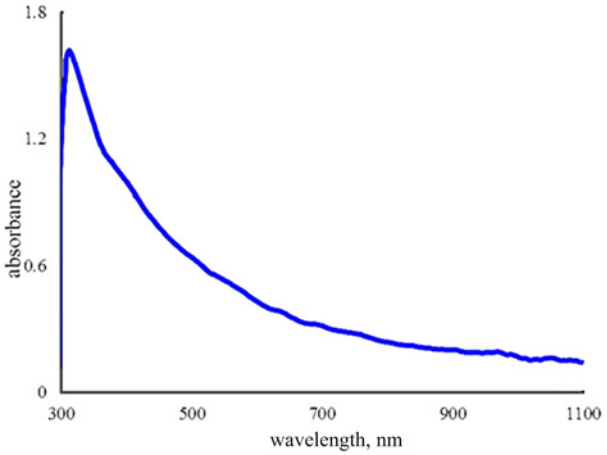

Fig. 2 *UV spectrum of PdNPs*

The schematic of the capacitor hydrogen sensor is shown in Fig. 3. For dry oxidation at first, cleans the thermal chemical vapour deposition furnace from other gases. Open nitrogen gas and ramp furnace up to 1000°C. In 1000°C temperature for 20 min the dry O_2 (2.5 l/min) will be opened. Over the oxide layer, a 100 nm film of PdNPs using the spin coating has been deposited. An Au film with thickness of 100 nm on the backside of the substrate using evaporating method has been coated. The atomic force microscope (AFM) image of oxide film surface is shown in Fig. 4. For oxidation time 20 min the oxide thickness is 50 nm. After oxidation, by AFM module (DS 95-50-E scanner) the surface properties of SiO_2 are characterised. The scan size at a resolution below 0.1 nm can be measured within the range of 50×50 µm. The average roughness is 3 nm.

The measurement set-up includes LCR meter modules (GPS-3135B) that can be interfaced to a PC. The frequency range of LCR meter is between 50 Hz and 100 kHz. The hydrogen absorption in the PdNPs has been investigated. Fig. 5 shows the set-up of volumetric method. In volumetric method using Sievert law, the ratio of hydrogen to the PdNPs (%) has been measured. The Sievert law can be readily rationalised by considering the reaction of dissolution of the gas in the metal, which involves dissociation of the gas molecules. The Sievert law is a rule to predict the solubility of gases in metals [18]. The ambient gases in the chamber using a vacuum pump are removed. The pressure changes due to absorption of hydrogen by the PdNPs in the chamber converts into an electrical signal using a transmitter.

3. Results and discussion: Fig. 6 shows the curve of pressure as a function of hydrogen concentration (wt%) in the PdNPs at room temperature. As indicated in Fig. 6, when pressure increases from 0.5 to 42 bar the ratio of hydrogen atom to PdNPs (wt%) is increased from 0.005 to 1%. The time for absorption is 110 s. Also, the curve of hydrogen desorption at room temperature has been shown in Fig. 6. The hydrogen desorption curve shows by decrease the pressure from 8 to 0.2 bar the ratio of hydrogen atom to PdNPs (weight%) decreases from 1 to 0.01%. The time for desorption is 150 s. When applied the positive voltage to the capacitor, electrons in Si are attracted to the Si–SiO_2 interface.

The capacitance of MOS capacitor for oxide thickness 50 nm is 69 nF. By applied negative voltage electrons in Si are repels from interface. In this depilation region, the capacitance can be obtained from [19]

$$C = (t_{ox}/\varepsilon_{ox}\varepsilon_0 A + X_d/\varepsilon_s\varepsilon_0 A)^{-1} \quad (1)$$

where ε_s is the semiconductor relative permittivity, ε_{ox} and t_{ox} are the relative permittivity and thickness of the oxide film, respectively, A is the area of the Pd gate and X_d is the thickness of the semiconductor depletion layer. By increase, the applied negative voltage the semiconductor enters an inversion layer. The capacitance before the inversion layer is 35 nF. In the MOS capacitor, the V_{FB} can be obtained from [19]

$$V_{FB} = (W_{MS}/q - Q/C_{ox}) \quad (2)$$

where W_{MS} is the work function difference between gate and substrate and Q is the trapped charges in the SiO_2 film [20]. For an ideal MOS capacitor the V_{FB} is zero, but for real MOS capacitor, the work function difference and trapped charges are not zero. For Pd, the work function is 5.2 eV and for semiconductor is 4.7 eV. The number of trapped charges for a MOS sensor is 2×10^{10} cm^{-2} [15]. For real Pd MOS capacitor sensor, the V_{FB} is 0.7 V. In the depletion layer, the capacitance can be achieved from [20]

$$C_T = C_{ox}\left(1 + 2\varepsilon_{ox}^2\varepsilon_0(V - V_{FB})/qN_D\varepsilon_s t_{ox}^2\right)^{-1/2} \quad (3)$$

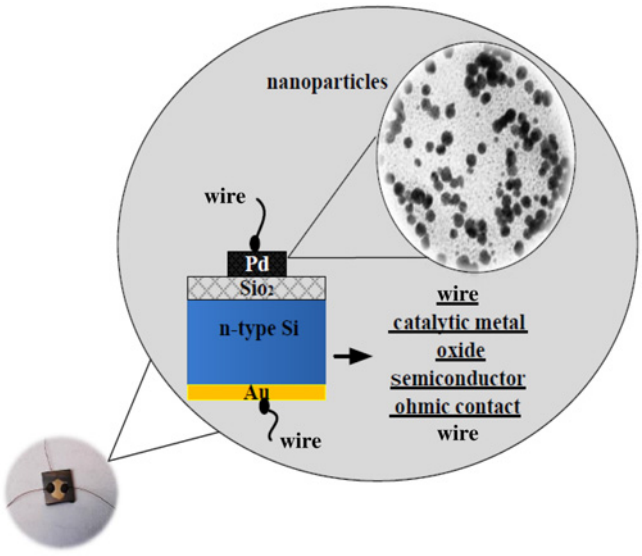

Fig. 3 *Schematic of the capacitor hydrogen sensor*

doi: 10.1049/mnl.2017.0586

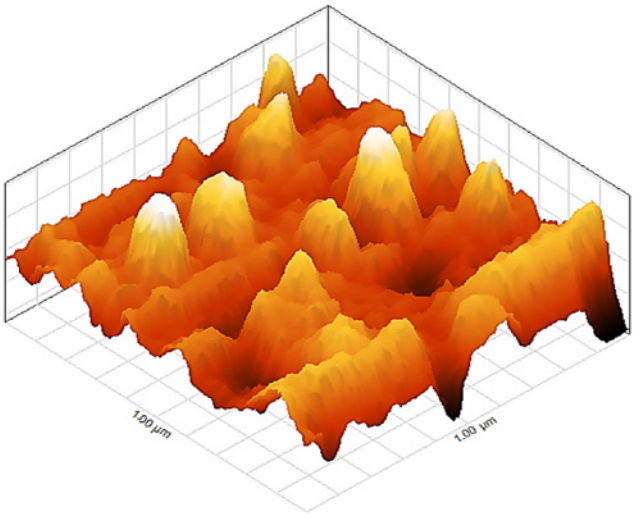

Fig. 4 *AFM image of the oxide film surface*

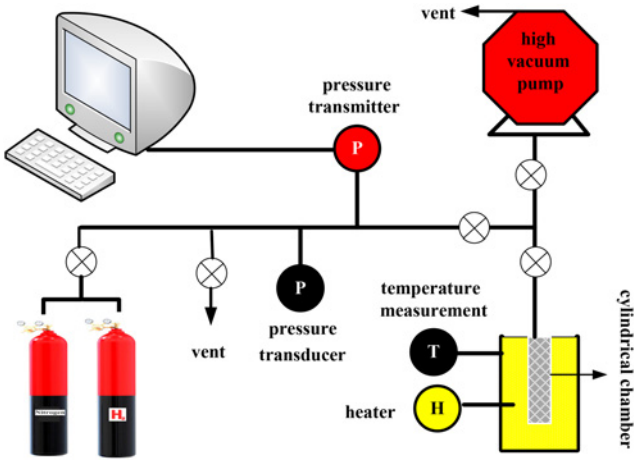

Fig. 5 *Measurement set-up for volumetric method*

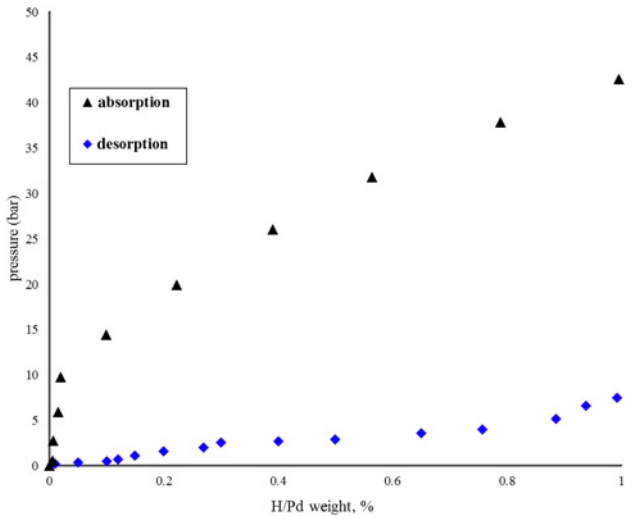

Fig. 6 *Pressure–concentration (P–C) curve of hydrogen absorption and desorption in the PdNPs at room temperature*

where N_D is the density of the donor carrier in the Si. Fig. 7 shows the comparison of *C–V* curves of ideal and real Pd MOS capacitor. From (3), in the depletion region by decreasing the capacitance

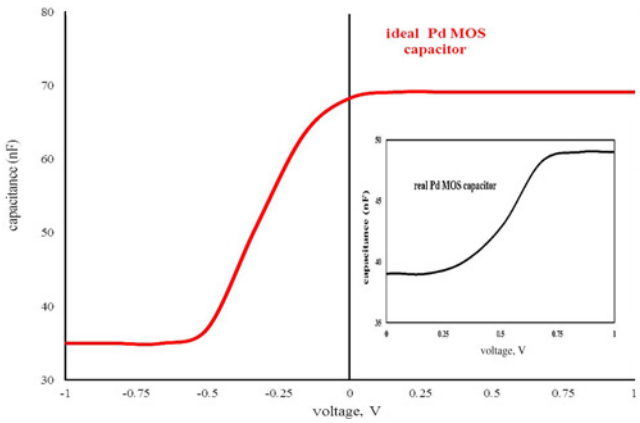

Fig. 7 *Comparison of C–V curves of ideal and real Pd MOS capacitor*

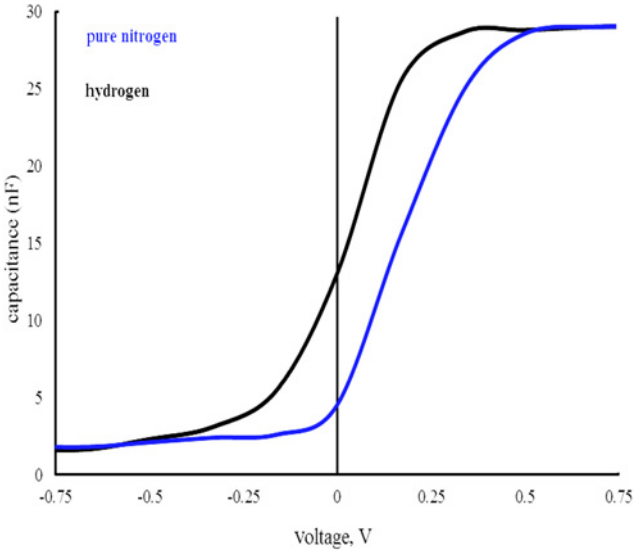

Fig. 8 *Experimental value of the C–V curves for the PdNPs MOS capacitor in pure nitrogen and 1% H_2–N_2 mixture*

from 69 to 35 nF the voltage of ideal Pd MOS capacitor decrease from 0 to −0.5 V. The relative permittivity of the SiO_2 is dependent to the frequency. By increasing the frequency from 1 to 100 kHz the permittivity decreases from 3.9 to 2.75. This difference is related to decrease of orienting of dipoles in the direction of the ac field. From (3), in the depletion region by decreasing the capacitance from 49 to 39 nF the voltage of real Pd MOS capacitor decrease from 0.7 to 0.2 V. As indicated in Fig. 6, in the accumulation and inversion layers, the capacitance is constant.

The experimental measurement of the *C–V* curves for the PdNPs MOS sensor in nitrogen and 1% H_2–N_2 mixture are shown in Fig. 8. The value of the V_{FB} for the real Pd MOS capacitor is 0.7 V and for experimental measurement (actual) in nitrogen is 0.5 V. The difference between real and actual MOS sensors is related to the trapped charges in the SiO_2 [19]. The trapped charges in the SiO_2 are caused a shift in the boundary between accumulation and depletion layers. From (2), when the SiO_2 trapped charges varies from 2×10^{10} to 8×10^{10} cm^{-2} the V_{FB} decreases from 0.7 to 0.5 V. It can be seen in Fig. 8, the *C–V* curve falls to the negative voltage when the nanosensor is exposed to the hydrogen. The V_{FB} decreases from 0.5 to 0.2 V. This decrease is due to the metal work function. At the Pd/SiO_2 interface, the dipole layer decreases the metal work function. Because of the work function change, the V_{FB} is shifted. Schematic of dipole layer in Pd/SiO_2 interface is shown in Fig. 9*a*. The mechanism of hydrogen detection is that of the association of hydrogen atoms at the metal/oxide interface. The dipole

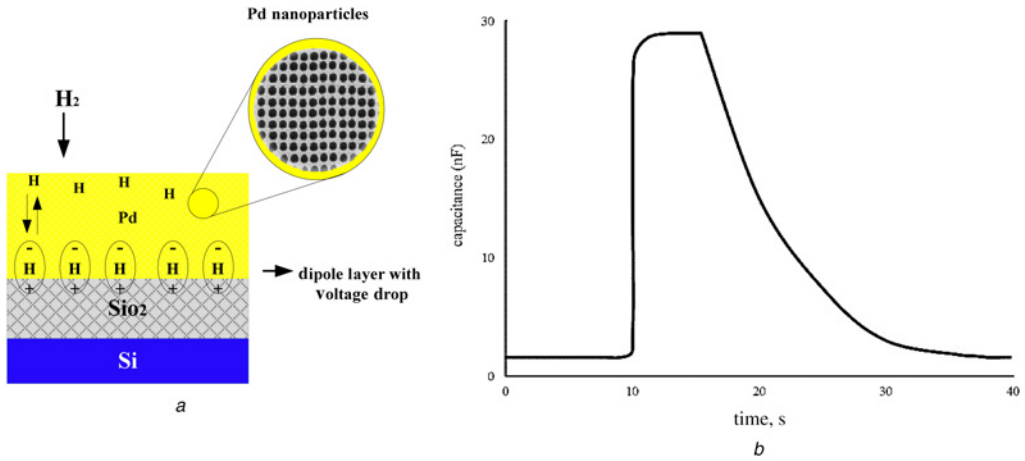

Fig. 9 *Schematic of*
a Dipole layer in Pd/SiO_2 interface
b Response and recovery times

Table 1 Comparison of MOS capacitive nanosensor hydrogen gas sensor and hydrogen sensors based on Pd

Material	Temperature range, °C	Detection limit, %	Physical sensing parameter	Response time, s	Recovery time, s	Reference
PdNPs	RT	1–4	MOS	1.4	14	this work
Pd–SiNWs–Schottky diode	RT	0.03–0.3	current	150	550	[28]
Pd–SiO_2–Si	RT	0.1–1.6	current	247	43	[29]
Pd–TiO_2–SiO_2–Si	RT	0.05–1	current	13	4	[30]
Pd–SiO_2	25–80	1	current	10	4	[31]
Pd–SnO_2	150–220	0.005–0.05	voltage	50	50	[32]
PdNPs–TiO_2 NTs	RT	1–5	conductance	120	90	[33]
Pd–Pt	150	1	resistance	4	5	[34]
Pd thin film	RT	0.04–1.6	resistance	25	10	[35]
PdNPs–SnO_2	200	0.001–0.3	resistance	4	10	[36]
PdNPs–MWCNTs	RT	6–30	resistance	15	20	[37]
PdNPs–SWCNTs	RT	0.01–1	resistance	$t_{36.8\%}=3$	300	[38]
PdNPs–graphene	30	2	resistance	6	56	[39]
Pd–Pt–Si nanowire	75	0–4	resistance	7.7	7.7	[40]

layer becomes stronger by an increase in the hydrogen atoms at the interface. The response of the nanosensor is obtained from [21–26]

$$R(\%) = (C_H - C_N)/(C_N) \times 100 \quad (4)$$

where C_H is the capacitance in a 1% H_2–N_2 and C_N is the capacitance in N_2. For the nanosensor, in the voltage 0.17 V, the response is 92%. The response and recovery times to 1% H_2–N_2 mixture at the 1.7 V voltage and 100 kHz frequency at 1 bar pressure in the room temperature are shown in Fig. 9*b*. The time interval to 90% of signal value ($t_{90\%}$) was 1.4 s. Our obtained results show the response of PdNPs nanosensor is faster than ultrathin Pd capacitor. The mechanism of nanosensor is that for small grain size, the work function change is huge [27]. Results indicate that the response time of nanosensor to be faster with PdNPs.

Comparison of different hydrogen gas sensors based on different physical sensing parameters is shown in Table 1. It can be seen in Table 1 the response time of MOS capacitive nanosensor is smaller than the current-based hydrogen gas sensors [28–31].

For voltage-based hydrogen gas sensor Pd/SnO_2 [32] the response and recovery times are 50 s. Table 1 shows for PdNPs/TiO_2 hydrogen gas sensor [33] at 50°C and 1–5% hydrogen concentration the response and recovery times are 120 and 90 s, respectively. Comparison of MOS capacitive nanosensor and resistance-based hydrogen gas sensors based on PdNPs and SnO_2/multi wall carb nanotubes (MWCNTs)/graphene/nanowire/single wall carbon nanotubes (SWCNTs) shows the response speed of MOS capacitive nanosensor is faster [34–40].

4. Conclusion: This Letter reported the effect of the PdNPs as a metal gate on the monitoring of hydrogen concentration by MOS nanosensor. The PdNPs MOS nanosensor showed sensitive and fast response/recovery times. The $t_{90\%}$ for 1% H_2–N_2 mixture was 1.4 s. The recovery time from 90 to 10% of signal value ($t_{10\%}$) was 14 s. Our obtained results in compared to ultrathin Pd sensor shows the response/recovery time of PdNPs nanosensor is faster. Also, in this Letter, the fabrication and characterisation (TEM and UV) of nanoparticles have been reported. The average size of nanoparticles is 9 nm. The curve of pressure as a function of hydrogen concentration (H/Pd) in the PdNPs shows the reversible ability of the nanosensor. Results indicate the response of MOS nanosensor has been improved with PdNPs as a metal gate.

5. Acknowledgement: This research work was supported by the Department of Physics, East Tehran Branch, Islamic Azad University, Tehran, Iran.

6 References

[1] Hubert T., Boon-Brett L., Black G., *ET AL.*: 'Hydrogen sensors – a review', *Sens. Actuators B*, 2011, **157**, pp. 329–352
[2] Buttner W.J., Post M.B., Burgess R., *ET AL.*: 'An overview of hydrogen safety sensors and requirements', *Int. J. Hydrog. Energy*, 2011, **36**, pp. 2462–2470

doi: 10.1049/mnl.2017.0586

[3] Boon-Brett L., Bousek J., Black G., *ET AL.*: 'Identifying performance gaps in hydrogen safety sensor technology for automotive and stationary applications', *Int. J. Hydrog. Energy*, 2010, **35**, pp. 373–384

[4] Ramanathan M., Skudlarek G., Wang H.H., *ET AL.*: 'Crossover behavior in the hydrogen sensing mechanism for palladium ultrathin films', *Nanotechnology*, 2010, **21**, p. 125501

[5] Khanuja M., Varandani D., Mehta B.R.: 'Pulse like hydrogen sensing response in Pd nanoparticle layers', *Appl. Phys. Lett.*, 2007, **91**, p. 253121

[6] Behzadi G., Golnabi H.: 'Comparison of invasive and non-invasive cylindrical capacitive sensors for electrical measurements of different water solutions and mixtures', *Sens. Actuators A, Phys.*, 2011, **167**, pp. 359–366

[7] Behzadi G., Golnabi H.: 'Monitoring temperature variation of reactance capacitance of water using a cylindrical cell probe', *J. Appl. Sci.*, 2009, **9**, pp. 752–758

[8] Behzadi G., Golnabi H.: 'Investigation of conductivity effects on capacitance measurements of water liquids using cylindrical capacitive sensor', *J. Appl. Sci.*, 2010, **10**, pp. 261–268

[9] Behzadi G., Fekri L., Golnabi H.: 'Effect of the reactance term on the charge/discharge electrical measurements using cylindrical capacitive probes', *J. Appl. Sci.*, 2011, **11**, pp. 3293–3300

[10] Behzadi G., Fekri L.: 'Electrical parameter and permittivity measurement of water samples using the capacitive sensor', *Int. J. Water Recourse Environ. Sci.*, 2013, **2**, pp. 66–75

[11] Lundstrom I., Shivaraman M., Svensson M., *ET AL.*: 'Hydrogen sensitive MOS field-effect transistor', *Appl. Phys. Lett.*, 1975, **26**, pp. 55–57

[12] Linke S., Dallmer M., Werner R., *ET AL.*: 'Low energy hydrogen sensor', *Int. J. Hydrog. Energy*, 2012, **37**, pp. 17523–17528

[13] Akbarzadeh A., Fekri Aval S., Sheervalilou R., *ET AL.*: 'Quantum dots for biomedical delivery applications', *Rev. Cell Biol. Mol. Med.*, 2016, **12**, pp. 66–76

[14] Fekri L., Jafari A., Fekri S., *ET AL.*: 'Comparison of synthesis and purification of carbon nanotubes by thermal chemical vapor deposition on the nickel-based catalysts: $NiSiO_2$ and 304-Type stainless steel', *J. Appl. Sci.*, 2010, **10**, pp. 716–723

[15] Basavegowda N., Mishra K., Rok Lee Y.: 'Green fabrication of ferromagnetic Fe_3O_4 nanoparticles and their novel catalytic applications for the synthesis of biologically interesting benzoxazinone and benzthioxazinone derivatives', *New J. Chem.*, 2014, **38**, pp. 5415–5420

[16] Yothi Kora A., Rastogi L.: 'Green synthesis of palladium nanoparticles using gum ghatti (*Anogeissus latifolia*) and its application as an antioxidant and catalyst', *Arab. J. Chem.*, 2015, in press

[17] Zhang G., Zhou H., Hu J., *ET AL.*: 'Pd nanoparticles catalyzed ligand-free Heck reaction in ionic liquid microemulsion', *Green Chem.*, 2009, **11**, p. 1428

[18] Sieverts A.: 'The absorption of gases by metals', *Zeitschrift für Metallkunde*, 1929, **21**, pp. 37–46

[19] Bentarzi H.: 'Transport in metal-oxide-semiconductor structure: mobile ions effects on the oxide properties' (Springer, New York, 2011), pp. 1–28

[20] Sze S.M.: 'Physics of semiconductor devices' (Willey, New York, 1987)

[21] Fekri Aval L., Elahi S.M., Darabi E., *ET AL.*: 'Comparison of the MOS capacitor hydrogen sensors with different SiO_2 film thicknesses and a Ni-gate film in a 4% hydrogen–nitrogen mixture', *Sensors and Actuators B: Chemical*, 2015, **216**, pp. 367–373

[22] Fekri Aval L., Elahi S.M.: 'Hydrogen gas detection using metal-oxide semiconductor capacitor with $Ni/SiO_2/Si$ structure'. IEEE Knowledge-Based Engineering and Innovation (KBEI), 2015, pp. 1133–1138

[23] Behzadi Pour G.: 'Electrical properties of the MOS capacitor hydrogen sensor based on the $Ni/SiO_2/Si$ structure', *J. Nanoelectron. Optoelectron.*, 2017, **12**, pp. 130–135

[24] Behzadi Pour G., Fekri Aval L.: 'Comparison of fast response and recovery Pd nanoparticles and Ni thin film hydrogen gas sensors based on metal-oxide-semiconductor structure', *NANO*, 2017, **12**, pp. 1750096-1–8

[25] Fekri Aval L., Elahi S.M.: 'Hydrogen gas detection using MOS capacitor sensor based on palladium nanoparticles-gate', *Electron. Mater. Lett.*, 2017, **13**, pp. 77–85

[26] Behzadi Pour G., Fekri Aval L.: 'Highly sensitive work function hydrogen gas sensor based on $PdNPs/SiO_2/Si$ structure at room temperature', *Results Phys.*, 2017, **7**, pp. 1993–1999

[27] Rakesh K.J., Krishnan S., Yoshimura M., *ET AL.*: 'Pd nanoparticles and thin films for room temperature hydrogen sensor', *Nanoscale Res. Lett.*, 2009, **4**, pp. 1191–1196

[28] Zhu L.S., Zhang J., Xu X.W., *ET AL.*: 'Room temperature H_2 detection based onPd/SiNWs/p-Si schottky diode structure', *Sens. Actuators B*, 2016, **227**, pp. 515–523

[29] Du Y., Xue Q., Zhang Z., *ET AL.*: 'Hydrogen gas sensing properties of $Pd/a\text{-}C:Pd/SiO_2/Si$ structure at room temperature', *Sens. Actuators B*, 2013, **186**, pp. 796–801

[30] Ling C., Xue Q., Han Z., *ET AL.*: 'High hydrogen response of $Pd/TiO_2/SiO_2/Si$ multilayers at room temperature', *Sens. Actuators B*, 2014, **205**, pp. 255–260

[31] Ohodnicki P.R., Baltrus J.P., Brown T.D.: 'Pd/SiO_2 and $AuPd/SiO_2$ nanocomposite-based optical fiber sensors for H_2 sensing applications', *Sens. Actuators B*, 2015, **214**, pp. 159–168

[32] Duy N.V., Toan T.H., Hoa N.D., *ET AL.*: 'Effects of gamma irradiation on hydrogen gas-sensing characteristics of $Pd\text{-}SnO_2$ thin film sensors', *Int. J. Hydrog. Energy*, 2015, **28**, pp. 12572–12580

[33] Xiang C., She Z., Zou Y., *ET AL.*: 'A room-temperature hydrogen sensor based on Pd nanoparticles doped TiO_2 nanotubes', *Ceramics Int.*, 2014, **40**, pp. 16343–16348

[34] Hassan K., Uddin A.S.M.I., Chung G.S.: 'Fast-response hydrogen sensors based on discrete Pt/Pd bimetallic ultra-thin films', *Sens. Actuators B*, 2016, **234**, pp. 435–445

[35] Hu Y., Lei J., Wang Z., *ET AL.*: 'Rapid response hydrogen sensor based on nanoporous Pd thin films', *Int. J. Hydrog. Energy*, 2013, **38**, pp. 313–318

[36] Li Y., Deng D., Chen N., *ET AL.*: 'Pd nanoparticles composited SnO_2 microspheres as sensing materials for gas sensors with enhanced hydrogen response performances', *J. Alloys Compd.*, 2017, **710**, pp. 216–224

[37] Zilli D., Bonelli P.R., Cukierman A.L.: 'Room temperature hydrogen gas sensor nanocomposite based on Pd-decorated multi-walled carbon nanotubes thin films', *Sens. Actuators B*, 2011, **157**, pp. 169–176

[38] Suna Y., Wang H.H.: 'Electrodeposition of Pd nanoparticles on single-walled carbon nanotubes for flexible hydrogen sensors', *Appl. Phys. Lett.*, 2007, **90**, p. 213107

[39] Kumar R., Malik S., Mehta B.R.: 'Interface induced hydrogen sensing in Pd nanoparticle/graphene composite layers', *Sens. Actuators B*, 2015, **209**, pp. 919–926

[40] Hassan K., Chung G.S.: 'Fabrication and characterization of fast response H_2 sensor based on Pd-Pt core-shell nanoparticles decorated Si nanowires cluster', *Procedia Eng.*, 2016, **168**, pp. 235–238